

Intraoperative Raman-Guided Chemo-Photothermal Synergistic Therapy of Advanced Disseminated Ovarian Cancers

Yuqing Zhang, Zhiyang Liu, Benjamin D. Thackray, Zhouzhou Bao, Xia Yin, Fenglei Shi, Jianbo Wu, Jian Ye,* and Wen Di*

Abdominal miliary spread and metastasis is one of the most aggressive features in advanced ovarian cancer patients. The current standard treatment of advanced ovarian cancer is cytoreductive surgery (CRS) combined with hyperthermic intraperitoneal chemotherapy (HIPEC). However, most patients cannot receive optimal CRS outcomes due to the extreme difficulty of completely excising all microtumors during operation. Though HIPEC can improve prognosis, treatment is untargeted and may damage healthy organs and cause complications. New strategies for precise detection and complete elimination of disseminated microtumors without side effects are therefore highly desirable. Here, cisplatin-loaded gap-enhanced Raman tags (C-GERTs) are designed specifically for the intraoperative detection and elimination of unresectable disseminated advanced ovarian tumors. With unique and strong Raman signals, good biocompatibility, decent plasmonic photothermal conversion, and good drug loading capacity, C-GERTs enable detection and specific elimination of microtumors with a minimum diameter of 1 mm via chemo-photothermal synergistic therapy, causing minimal side effects and significantly prolonging survival in mice. The results demonstrate that C-GERTs-based chemo-photothermal synergistic therapy can effectively control the spread of disseminated tumors in mice and has potential as a safe and powerful method for treatment of advanced ovarian cancers, to improve survival and life quality of patients.

1. Introduction


Ovarian cancer is one of the major causes of gynecologic cancer-related mortality, with increasing rates of occurrence in recent years.^[1,2] Global cancer statistics show that ≈238 700 new ovarian cancer cases and 151 900 deaths occurred in 2012 worldwide.^[3] 80% of recorded ovarian cancer patients have epithelial ovarian cancer (EOC) and most are diagnosed at an advanced stage. Consequently, the 5 year survival rate is less than 30%.^[4–8] The current standard treatment of advanced stage EOC consists of cytoreductive surgery (CRS) and platinum-based (e.g., cisplatin) chemotherapies.^[9–11] For optimal CRS in patients with advanced stage cancer, clinicians will usually remove the primary ovary, together with the whole uterus, double attachments, pelvic metastasis nodules, and even part of the bowel if metastasis is diagnosed.^[12,13] Despite this significant resection, most patients with advanced EOC do not in

Dr. Y. Zhang, Dr. B. D. Thackray, Prof. J. Ye
School of Biomedical Engineering
Shanghai Jiao Tong University
Shanghai 200030, P. R. China
E-mail: yejian78@sjtu.edu.cn

Dr. Z. Liu, Z. Bao, Dr. X. Yin, Prof. W. Di
Department of Obstetrics and Gynecology
Ren Ji Hospital
School of Medicine
Shanghai Jiao Tong University
Shanghai 200127, P. R. China
E-mail: diwen@renji.com

Dr. Z. Liu, Z. Bao, Dr. X. Yin, Prof. W. Di, Prof. J. Ye
Shanghai Key Laboratory of Gynecologic Oncology
Ren Ji Hospital
School of Medicine
Shanghai Jiao Tong University
Shanghai 200127, P. R. China

Dr. Z. Liu, Z. Bao, Dr. X. Yin, Prof. W. Di, Prof. J. Ye
State Key Laboratory of Oncogenes and Related Genes
Shanghai Cancer Institute
Ren Ji Hospital
School of Medicine
Shanghai Jiao Tong University
Shanghai 200127, P. R. China
F. Shi, Prof. J. Wu
State Key Laboratory of Metal Matrix Composites
School of Materials Science and Engineering
Shanghai Jiao Tong University
Shanghai 200240, P. R. China

 The ORCID identification number(s) for the author(s) of this article can be found under <https://doi.org/10.1002/sml.201801022>.

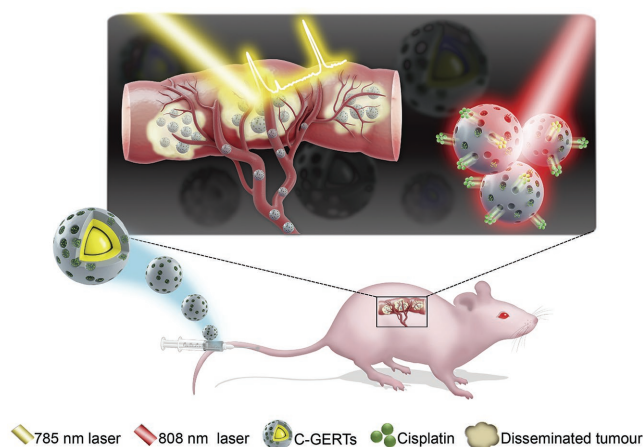
DOI: 10.1002/sml.201801022

practice receive optimal CRS outcomes due to the extreme difficulty of completely excising all microtumors less than 1 cm during operation,^[14,15] which typically exhibit numerous miliary nodules diffused in the peritoneum,^[16,17] intestinal canal, and abdominal viscera.^[18–20] Postoperative chemotherapy is often used to attack unresectable cancer cells.^[21] However, patients frequently relapse during the course of treatment due to cisplatin resistance.^[22,23]

Recent research suggests that optimal CRS combined with hyperthermic intraperitoneal chemotherapy (HIPEC) may be the best treatment choice for advanced ovarian cancer and prolonged survival.^[24–27] Though HIPEC can improve prognosis, it has limitations. Since HIPEC acts on all the organs in the abdominal and pelvic cavity with no tumor targeting effect, it will inevitably damage normal organs and can cause complications including intestinal adhesion and obstruction.^[28] In addition, the cycle time of treatment and perfusion are both long, some patients are intolerant of therapy and have to discontinue treatment.^[28] It is believed that patient survival rates can be greatly improved if we can target hyperthermia and chemotherapy to miliary unresectable tumors locally and specifically. New strategies for precise detection and complete elimination of disseminated microtumors without causing side effects are therefore highly desirable.

Surface-enhanced Raman scattering (SERS)–based detection is a promising approach for identifying microtumors with higher specificity and sensitivity than other intraoperative imaging techniques (e.g., magnetic resonance imaging (MRI), fluorescence, and ultrasound).^[29–31] Using the unique “fingerprint” signals of Raman probes, tumors containing probes can be distinguished from the surrounding normal tissues specifically. SERS imaging has been successfully used to detect tumor margins and guide the resection of bulk tumors with one or several lesions,^[32–34,37] though no currently published studies demonstrate its application for complete detection and removal of numerous microtumors spread in the abdominal cavity, a key feature of advanced stage ovarian cancer. Furthermore, most SERS nanoprobe are made from metals such as gold and silver, which typically possess high photothermal conversion efficiency. This photothermal effect can be exploited to design ultrasensitive SERS nanoprobe that combine diagnostic detection with photothermal- and chemotherapy to both detect and then eliminate disseminated microtumors completely.

In this study, we use mouse models with millet-shaped disseminated microtumors in their abdominal cavity in order to better mimic the clinical status of advanced ovarian tumor patients after receiving the best possible CRS. We develop multifunctional SERS nanoprobe, cisplatin-loaded gap-enhanced Raman tags (C-GERTs), specifically for the intraoperative detection and elimination of unresectable disseminated advanced ovarian tumors (**Scheme 1**). C-GERTs are core-shell gold nanoparticles (NPs) with embedded Raman reporters and an external mesoporous silica layer loaded with cisplatin, one of the preferred chemotherapeutic drugs for ovarian cancer in clinic. In addition to their decent plasmonic photothermal conversion capacity, GERTs possess a number of other advantages: i) a unique “fingerprint” Raman signal from the molecules inside the nanogaps, which is easily distinguished from biological tissues; ii) strong enhancement of this signal by the



Scheme 1. Raman-guided detection and chemo-photothermal synergistic therapy of abdominal disseminated microtumors with cisplatin-loaded gap-enhanced Raman tags (C-GERTs). The tumors on the intestine represent advanced disseminated ovarian microtumors.

core-shell particle, for detecting microtumors with a high sensitivity; iii) good biocompatibility of the external mesoporous silica layer, which additionally serves as a drug loading site. Combining all these features, we designed C-GERTs for advanced ovarian cancer patients with multiple microtumor lesions, to identify and treat all lesions quickly and effectively. In this study, we assess the feasibility of C-GERTs for Raman-based detection of microtumors with a minimum diameter of 1 mm, and then perform local photothermal- and chemotherapy simultaneously, to eliminate disseminated microtumors specifically and with minimal side effects. We continue to monitor the therapeutic effect for more than 20 days after treatment, to fully compare different treatment methods. In addition, the cytotoxicity of C-GERTs and their in vivo influence on body weight, blood biochemistry, and important organs are all evaluated for future clinical applications.

2. Results

2.1. Characterization of C-GERTs

GERTs composed of a gold (Au) core, sub-nanometer gap containing reporter molecules, Au shell, and external mesoporous silica layer (inset in **Figure 1a**) were synthesized according to the optimized procedure previously described.^[35,36] The core-shell structure of the GERTs is clearly seen in transmission electron microscopy (TEM) imaging, where we measure a built-in gap size of 0.7–1.0 nm, a mesoporous silica layer thickness of 13 ± 3 nm, and a total particle size of 84 ± 4 nm (**Figure 1a(i)**). The internal gap size is mainly determined by the self-assembly of the embedded 1,4-benzenedithiol (1,4-BDT) Raman reporters, which may form a monolayer or multilayer structure.^[36,37] C-GERTs (**Figure 1a(ii)**) are obtained by loading cisplatin into the pores of the external mesoporous silica layer, facilitated by the pendent carboxylic groups on the silica surface which act as bonding sites.^[38] Loading efficiency as high as 51.2% was measured by atomic adsorption spectrometry.

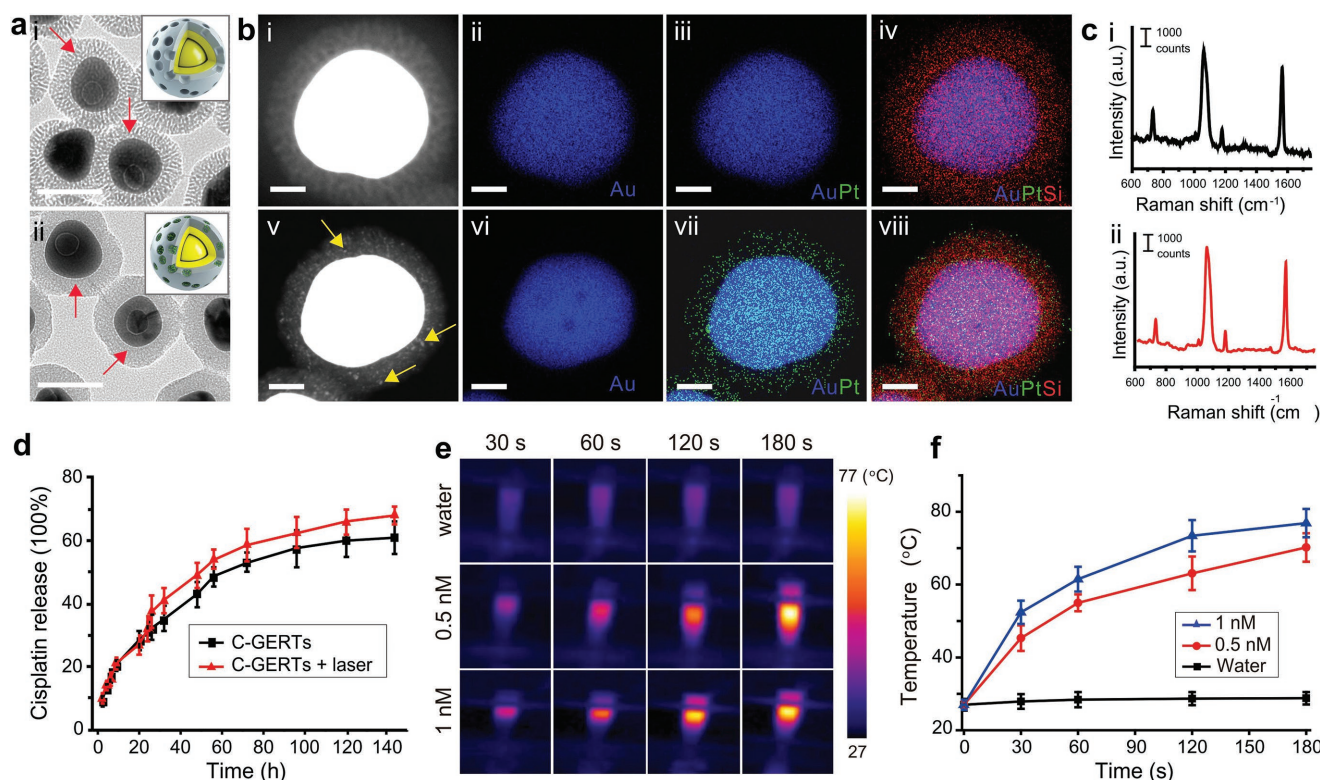


Figure 1. Unique structure and properties of cisplatin-loaded GERTs (C-GERTs). a) Representative transmission electron microscopy (TEM) images of GERTs (i) and C-GERTs (ii). Insets show the corresponding schematic illustrations of GERTs and C-GERTs. The silica layer before and after cisplatin loading is indicated by red arrows. b) HAADF-STEM images, EDS elemental mapping images of Au, overlay of Au and Pt, and overlay of Au, Pt, and Si of GERTs (i–iv) and C-GERTs (v–viii). All scale bars are 50 nm. Pt element in HAADF-STEM image is indicated by yellow arrows. c) Raman spectra of GERTs (i) and C-GERTs (ii). d) Releasing behavior of cisplatin from the C-GERTs with and without near-infrared (NIR) laser irradiation at the 24 h time point. e) In vitro NIR thermographic images and f) the temperature elevation of aqueous C-GERTs with different concentrations and time intervals.

The silica pores appeared obscured in TEM images after drug loading (indicated by the red arrows in Figure 1a(i),(ii)) showing the successful loading of cisplatin. Energy dispersive spectrometer (EDS) elemental mapping performed by high-angle annular dark-field scanning TEM (HAADF-STEM) further demonstrates the loading of cisplatin into the silica layer by considering the constituent variation of GERTs in terms of the spatial distribution of the element of Au (from Au core and Au shell), Si (solely from the mesoporous silica layer), and Pt (solely from cisplatin) (Figure 1b). HAADF-STEM images also show the distribution of Pt element in the silica layer after cisplatin loading (indicated by yellow arrows and green color in Figure 1b(v),(vii)), while no Pt element appears before loading (Figure 1b(i),(iii)). In addition, the absorbance of the supernatant after loading process is significantly reduced compared to initial cisplatin solution (Figure S1a, Supporting Information). After cisplatin loading, it can be noticed that the hydrodynamic size increases slightly from 105 (GERTs) to 122 nm (C-GERTs) (Figure S1b, Supporting Information), indicating that cisplatin is loaded not only in the pores but also on the surface of the silica layer. The zeta potential (Figure S1c, Supporting Information) also changes from -23 (GERTs) to -13.4 mV (C-GERTs) after cisplatin loading due to partial replacement of carboxyl groups by cisplatin on the surface of silica layer. All these results demonstrate the successful loading of cisplatin. Importantly, the strong Raman signal is not significantly affected

by the cisplatin loading in the mesoporous silica layer (Figure 1c(i),(ii)). Two strong characteristic Raman bands of GERTs and C-GERTs at 1055 and 1555 cm^{-1} and two weak bands at 732 and 1178 cm^{-1} correspond to the phenyl-ring breathing mode (C–H in-plane bending and C–S stretching), the phenyl-ring stretching motion (8a vibrational mode), and the CH bending motion (9a vibrational mode), respectively.

To investigate their drug releasing behavior, two groups of C-GERTs were immersed in phosphate buffered solution (PBS, pH = 7.0) at 37 °C and time-dependent drug releasing profiles were recorded. In the first 24 h, cisplatin was passively released by both groups. After 24 h, a laser (808 nm, 3 W cm^{-2} , 5 min) was applied to the “C-GERTs + laser” group. After that, cisplatin of both groups continued to release freely. The release profiles of both groups (Figure 1d) show slow and sustained patterns within the first 24 h without a burst releasing effect, which is unavoidable with traditional cisplatin administration. Differences in release efficiency of the C-GERTs (31.05%) and C-GERTs + laser (32%) groups in the first 24 h were negligible. During laser irradiation at the 24 h time point, cisplatin is released slightly faster from the C-GERTs + laser group than from the C-GERTs group, with cumulative release efficiencies of 68% and 61%, respectively, over the next 4 days. Although the plasmon resonance peaks of GERTs and C-GERTs are both in the range of 540 – 550 nm (Figure S2a, Supporting Information), we choose 808 nm

laser for photothermal treatment considering the in vivo application. Under continuous laser irradiation (808 nm , 3 W cm^{-2}), C-GERTs exhibit decent photothermal effect. In Figure 1e,f, the temperature of the C-GERT suspension shows an obvious elevation from 27 to 72.4 and $76.5\text{ }^{\circ}\text{C}$ in 3 min , at concentrations of 0.5×10^{-9} and $1 \times 10^{-9}\text{ M}$, respectively. In contrast, water exhibits negligible temperature increase under the same experimental conditions. The photothermal conversion efficiency (η) was about 33% based on our calculations (Figure S2b,c, Supporting Information) according to Roper et al.'s method.^[39] In addition, the probes show excellent SERS-based imaging and detection capabilities for cells and tumors (Figure S3, Supporting Information), which act as a promising candidate for in situ Raman detection-guided photothermal therapy of tumors.

2.2. In Vitro Chemo-Photothermal Therapy Effects

Cytotoxicity of GERTs was evaluated in vitro by cell counting kit-8 (CCK-8) assay and the results show negligible cytotoxicity of GERTs when cocultured with SKOV3 cells, even after 72 h at concentrations up to $0.2 \times 10^{-9}\text{ M}$ (Figure 2a). The effects of chemo-photothermal therapy with GERTs on cell

viability in vitro can be seen in Figure 2b,c. Fluorescence imaging in Figure 2b clearly indicates that almost all cells in the laser group remain alive (calcein-AM stained, green) after 5 min of irradiation treatment (808 nm , 3 W cm^{-2}), whereas about 20% of cells in the C-GERT group appear dead (propidium iodide (PI) stained, red) without irradiation, due to the chemotherapeutic effect of cisplatin ($0.1 \times 10^{-9}\text{ M}$). However, about 90% cells of GERTs + laser group ($0.1 \times 10^{-9}\text{ M}$, 3 W cm^{-2}) appear dead after laser irradiation due to the photothermal effect. Moreover, almost 100% of cells in the C-GERTs + laser group ($0.1 \times 10^{-9}\text{ M}$, 3 W cm^{-2}) are killed by chemo-photothermal synergistic therapy. These results are confirmed by the cell viabilities of the C-GERTs, GERTs + laser, and C-GERTs + laser groups shown in Figure 2c, which are $81.75 \pm 4.04\%$, $11.75 \pm 2.24\%$, and $0.5 \pm 0.22\%$, respectively. Consequently, we learn that the photothermal effect plays a more important role than the chemotherapeutic effect for killing the SKOV3 cells. We also find that the concentration of C-GERTs and the laser power density can affect the therapeutic effects. For example, when the concentration of C-GERTs is decreased from 0.1×10^{-9} to $0.05 \times 10^{-9}\text{ M}$ or the laser power density is decreased from 3 to 2 W cm^{-2} , more cells survive (Figure S4, Supporting Information). Our results demonstrate that the C-GERTs + laser group shows a

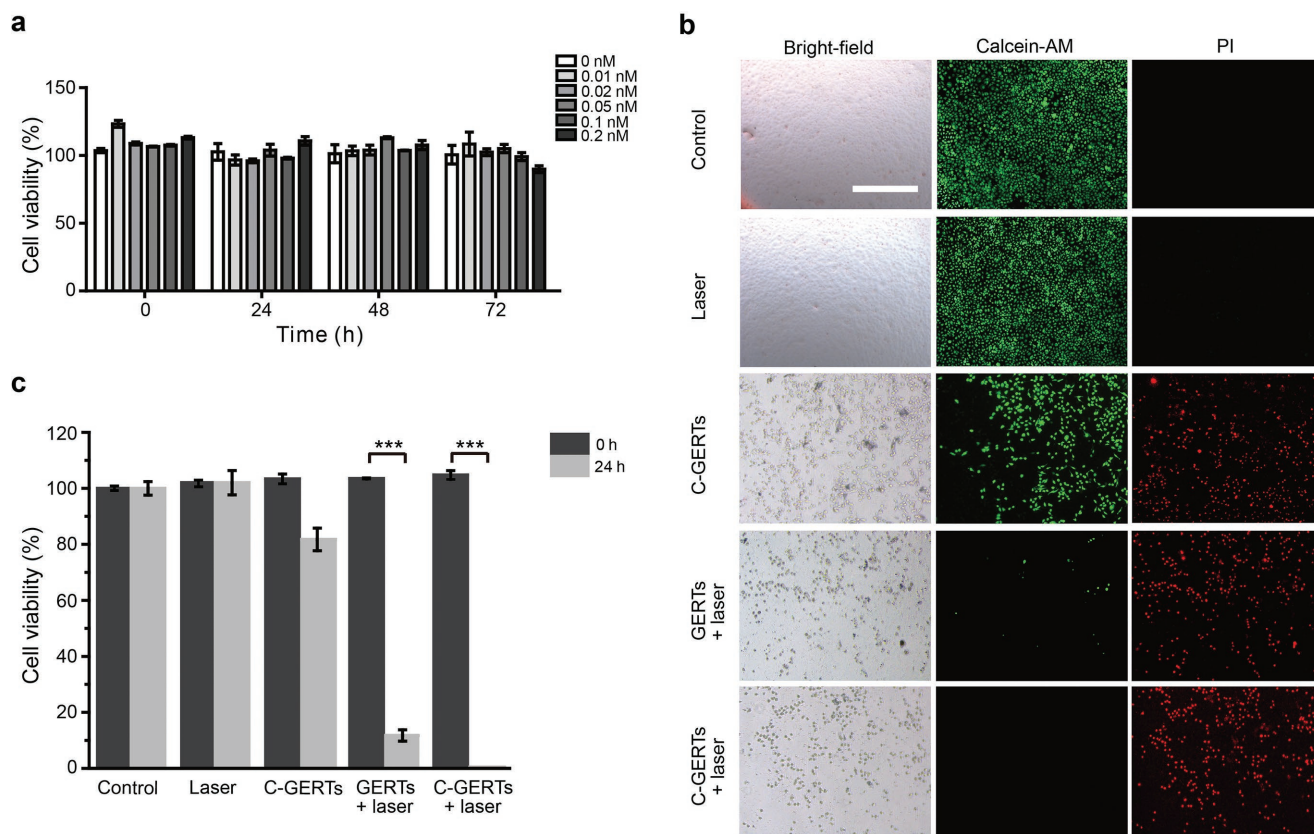


Figure 2. In vitro cellular chemo-photothermal synergistic therapy. a) Cellular viability of SKOV3 cells incubated with GERTs at different concentrations for 24 , 48 , and 72 h . Data are shown as mean \pm SD. b) Bright-field and fluorescent images of SKOV3 cells treated with different conditions. All concentrations of nanoprobe were $0.1 \times 10^{-9}\text{ M}$, laser power was 3 W cm^{-2} , and irradiation time was 5 min . The cells were stained with calcein-AM (live: green) and PI (dead: red). The scale bar is $500\text{ }\mu\text{m}$. c) Cell viability of SKOV3 cells treated with different conditions in (b). Data are represented as mean \pm standard deviation ($n = 6$). Significant differences are indicated by asterisks ($***p < 0.001$).

synergistic chemo-photothermal therapeutic effect on SKOV3 cells.

2.3. Intraoperative Real-Time Raman Detection and Chemo-Photothermal Therapy of Disseminated Ovarian Microtumors

Investigation of blood circulation time and biodistribution of C-GERTs show that 24 h after injection is the appropriate detection and treatment time and C-GERTs exhibit a decent passive targeting capability to tumors (Figure S5, Supporting Information). GERTs and C-GERTs were tail vein injected for the C-GERTs,

GERTs + laser, and C-GERTs + laser groups to help detect and cure disseminated microtumors. All mice were anesthetized and underwent aseptic laparotomy surgery 24 h after injection, with disseminated tumors in the abdominal cavity identified with the Raman system. During laparotomy surgery of the five groups (saline, cisplatin, C-GERTs, GERTs + laser, and C-GERTs + laser) in vivo, we could easily detect the intrinsic 1,4-BDT Raman signals from disseminated microtumors of mice in the C-GERTs, GERTs + laser, and C-GERTs + laser groups (Figure S6, Supporting Information). We presume that GERTs accumulate in the tumors mainly via the enhanced permeability and retention (EPR) effect.^[40,41] Different sizes of disseminated microtumors

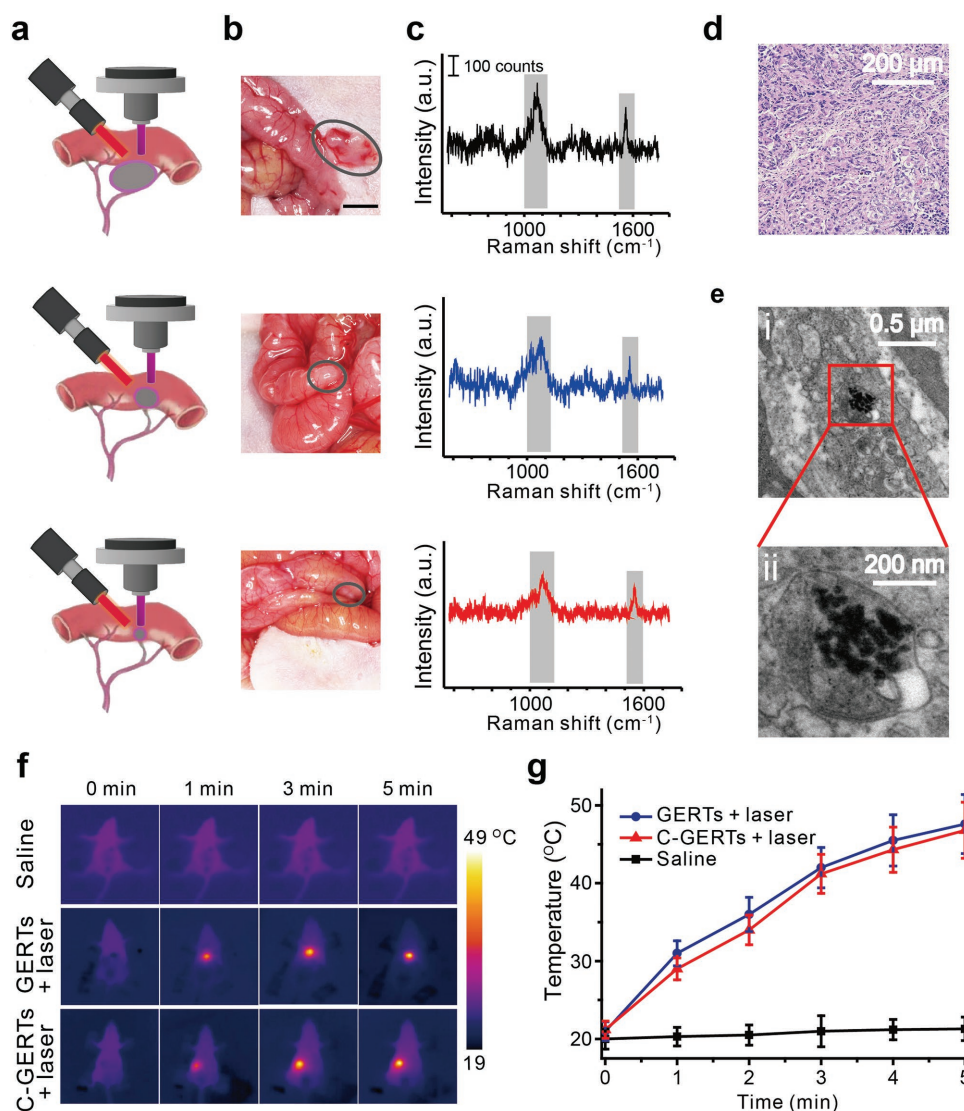


Figure 3. In vivo intraoperative Raman-guided chemo-photothermal therapy of advanced ovarian cancers with disseminated microtumors. a) Schematic diagrams of the intraoperative detection of microtumors (of various sizes) guided by Raman spectroscopy and localized chemo-photothermal therapy performed by NIR laser radiation. b) Representative images of disseminated tumors (indicated by the gray circles) of different diameters on the intestine and intestinal mesentery (top: 0.7 cm, middle: 0.35 cm, and bottom: 0.1 cm) and c) the corresponding detected Raman signals. The scale bar is 200 counts. d) Representative histological analysis of microtumors obtained from mice and e) representative TEM images showing the presence of C-GERTs within the tumor cell. f) NIR intraoperative thermographic images and g) the temperature change curves of mice injected by saline, GERTs, and C-GERTs, with microtumor sites guided by Raman signals of GERTs upon 808 nm laser irradiation (3 W cm^{-2} , 5 min, laser point of 5 mm in diameter).

could be identified during the operation and the superhigh specificity and sensitivity of C-GERTs allowed us to easily locate microtumors with sizes as small as 0.1 cm in diameter (Figure 3a,b). As shown in Figure 3b,c, characteristic Raman signals of C-GERTs at 1055 and 1555 cm^{-1} could be easily detected from various sizes of tumors (0.1–0.7 cm in diameter) within 5 s using a Raman scanner. These tiny tumor sites are often indistinguishable to the naked eye and are therefore very commonly overlooked in ovarian cancer surgery. For the locations with positive Raman signals, pathology examination confirmed the existence of the epithelial ovarian cancer cells (Figure 3d). In addition, TEM measurements from the locations with Raman positive signals provide further evidence of the accumulation of C-GERTs in tumor cells (Figure 3e) and it is notable that loading of GERTs with cisplatin does not appear to affect their accumulation in tumor cells compared to unloaded GERTs (Figure S7, Supporting Information). Subsequently, we performed real-time near-infrared (NIR) photothermal therapy (808 nm, 3 W cm^{-2}) on the positive Raman locations. For the GERTs + laser and C-GERTs + laser groups, the temperature at the irradiated tumor focus increased remarkably from ≈ 21 to ≈ 42 °C in 3 min (Figure 3f,g) and continued to rise to ≈ 47 °C in 5 min. These results from real-time temperature monitoring indicate that nanoprobe accumulated in the tumor focus are capable of generating sufficient heat for tumor ablation (usually >42 °C) upon NIR laser irradiation. In contrast, the saline group showed negligible temperature increase of ≈ 1 °C after the same laser irradiation treatment, indicating that such NIR laser power density does not cause thermal damage to normal tissues. Additionally, the laser spot size can be adjusted according to the actual situation during treatment. For example, if several tumor foci are located close to each other, we can increase the laser spot size and treat them together to shorten the operation time.

2.4. In Vivo Therapeutic Effect Evaluation after Chemo-Photothermal Therapy

The in vivo therapeutic effects of our different intraoperative techniques were evaluated by continuously monitoring the regrowth and spread of tumors for 20 days post-treatment using bioluminescence signals. As shown in Figure 4, mice in the saline group exhibited sustained growth of tumor volumes, and tumors spread to the entire abdominal cavity within 20 days (Figure 4a), with the corresponding total flux (TF) value of tumors increasing to more than 600% of the initial value (Figure 4b). This indicates rapid growth of the ovarian tumors. For the

free cisplatin group, the tumors showed a dramatic reduction in size 4 days after treatment, but exhibit uncontrolled growth and disseminate throughout the entire peritoneal cavity after 10 days (Figure 4a), with TF value also as high as 600%, 20 days after treatment (Figure 4b). This indicates that a single low dose of cisplatin can only suppress tumor growth for a short period of time, and cannot completely eliminate tumors. After cisplatin is metabolized, the tumors tend to relapse rapidly. For the C-GERTs group, C-GERTs loaded with cisplatin can passively target to tumor foci and release drugs slowly and locally. During the observation period, tumor size shows

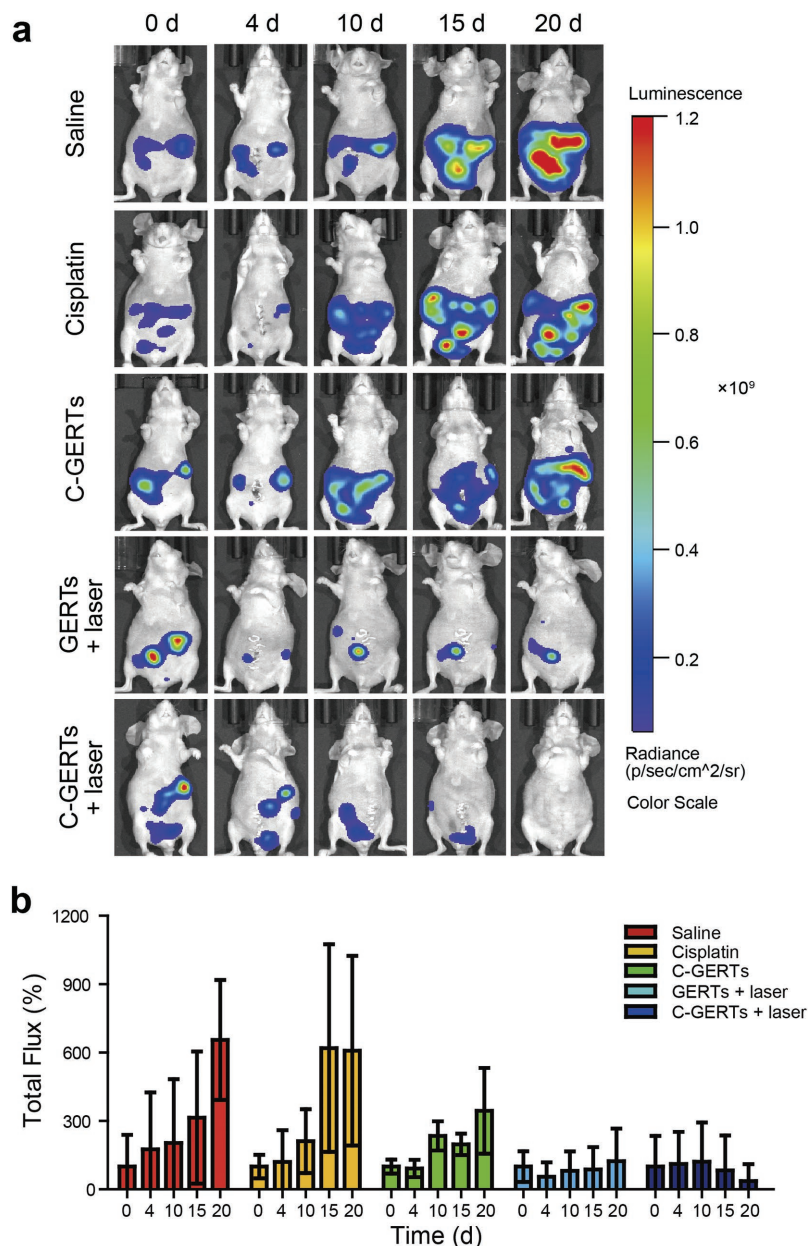


Figure 4. Bioluminescence monitoring of therapeutic effect after treatment of disseminated tumors. a) Representative bioluminescent images of regrowth and dissemination of SKOV3_{luc} tumors in each group after treatment. The bioluminescence signals of mice were continuously monitored for 20 days. b) Tumor growth profiles of mice of five groups according to the total bioluminescence value of each groups. Values are shown as the mean \pm SD ($n = 5$).

a similar initial trend to the cisplatin group due to the chemotherapy effect of the slowly released cisplatin, but the regrowth rate of tumors is much slower than that of the cisplatin group, with a maximal TF value of about 300% 20 days after treatment. Comparatively, the tumors of mice in the GERTs + laser group appear to be suppressed for the first 15 days after operation with average TF value lower than the initial value. However, tumors show likely recurrence by the 20th day. The C-GERTs + laser group shows the best therapeutic effect, with near complete elimination of tumors and suppression of regrowth;

average TF value decreased to about 37% 20 days after treatment. Although the measured average TF values were not yet obviously reduced by the 10th and 15th day, it is clear in Figure 4a that the tumor range has been effectively contained. These results provide strong evidence that Raman-guided localized chemo-photothermal treatment with C-GERTs can kill tumor cells and effectively prevent disseminated tumor recurrence.

The extent of tumor dissemination in the abdominal cavities of mice from the five groups 20 days after treatment is carefully

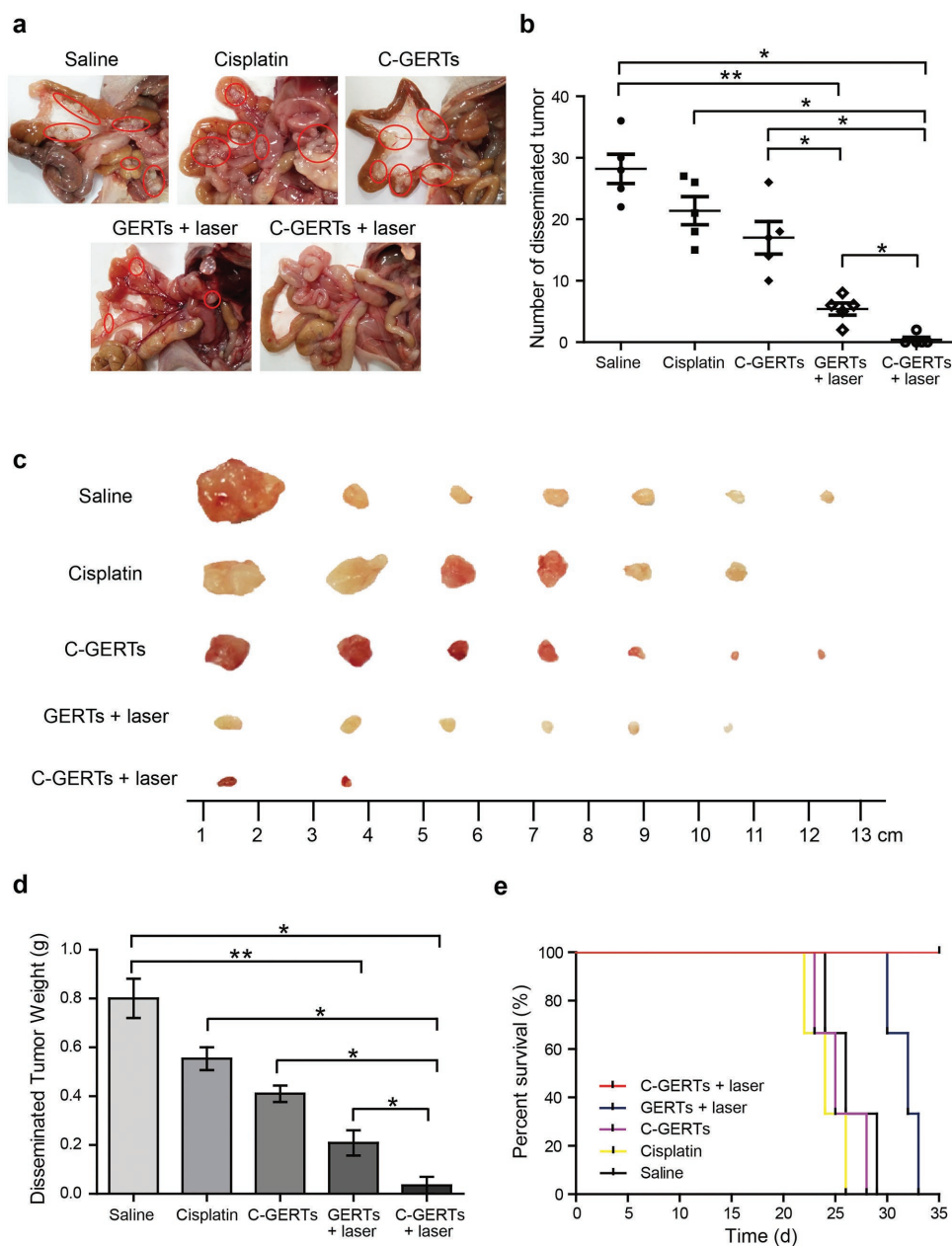


Figure 5. Evaluation of the therapeutic effects after different treatments of disseminated ovarian tumors. a) Representative photographs of tumors 20 days after treatment. The red circles indicate the intra-abdominal disseminated tumors. b) The number of tumors per mouse for each group ($n = 5$). c) Representative photograph of disseminated tumors in each group at the end of the experiment. d) Weight of disseminated tumors per mouse, and values are shown as the mean \pm SD. Significant differences are indicated by asterisks. $^{**}p < 0.01$; $^{*}p < 0.05$. e) Overall survival curves of the five treatment groups.

examined in **Figure 5a**. In the saline, cisplatin, and C-GERTs groups, a number of large tumors spread over the intestine and mesentery; and in the GERTs + laser group, only a few small tumors remained; however in the C-GERTs + laser group, most of the mice were cured. As shown in **Figure 5b**, the average number of disseminated mesenteric tumors found in mice in the saline, cisplatin, and C-GERTs group 20 days after treatment is 28, 21, and 17 per mouse, respectively. Mice in the GERTs + laser group were found to have comparatively few small intra-abdominal tumors (5 per mouse). In the C-GERTs + laser group, 80% of mice were completely cured, with just 2 mice found to have 1 small tumor remaining each. Furthermore, the size of disseminated tumors after treatment from the five groups was also measured; tumors in the C-GERTs + laser group (<0.3 cm in diameter) were much smaller than those in other four groups, which were sometimes larger than 1 cm in diameter (**Figure 5c**). Compared with tumor weights in the saline + laser, cisplatin, C-GERTs, and GERTs + laser groups ($\approx 0.80 \pm 0.14$, 0.55 ± 0.08 , 0.41 ± 0.06 , and 0.18 ± 0.15 g per mouse, respectively), the average tumor weight in the C-GERTs + laser group was significantly reduced to 0.03 ± 0.05 g per mouse (**Figure 5d**). It is worth noting that there was also significant reduction in tumor number, size, and weight in the GERTs + laser group, when compared with the groups with non-GERT-based treatment. The above results demonstrate the effectiveness of C-GERTs + laser- and GERTs + laser-based treatments to inhibit the regrowth of disseminated ovarian cancer in vivo, which is consistent with our results in vitro (**Figure 2b,c**). Survival curves of mice in five groups further demonstrate their therapeutic effects (**Figure 5e**). The C-GERTs + laser group achieves a survival rate of 100% during the observation period (35 days). In contrast, all mice in the other four groups eventually succumbed to their tumors, with survival times of 26.33 ± 2.05 , 24 ± 1.63 , 25.33 ± 2.05 , and 31.67 ± 1.25 days for saline + laser, cisplatin, C-GERTs, and GERTs + laser groups, respectively.

2.5. In Vivo Biocompatibility Study of C-GERTs

Histological analysis of major organs (liver, lung, kidney, heart, and spleen) shows no noticeable irregularities in tissue structures in the experimental groups when compared with the control group, suggesting that no obvious signs of toxicity are found in the harvested organs (**Figure 6a**). Although cisplatin is one of the most effective anticancer agents and widely used clinically to fight ovarian cancer, nephrotoxic side effects are commonly observed in cancer patients. For this reason, we also studied liver and kidney functions to evaluate the toxicity of C-GERTs. It is known that inflammatory and oxidative response can be detected by serum analysis. Serum protein analysis results are shown in **Figure 6b–e**; among them, alanin transaminase (ALT) and aspartate aminotransferase (AST) levels are used to assess liver toxicity, creatinine (CREA) and urea levels are used to assess kidney toxicity. Fortunately, all four indicators show no significant differences between experimental groups and the control group. This indicates that GERTs and C-GERTs are minimally toxic to the liver and spleen, which further confirms the histology results (**Figure 6a**).

Additionally, body weight curves of five groups show little difference (**Figure 6f**), indicating no obvious toxicity of GERTs and C-GERTs in vivo. The initial slight weight loss of all groups may be due to the surgery wound. All our in vitro experiments (**Figure 2a**) and in vivo experiments (**Figure 6**) demonstrate that GERTs and C-GERTs have good biocompatibility.

3. Discussion

As we have emphasized, the major challenge presented by advanced stage ovarian cancer is the extreme difficulty of exhaustively identifying and destroying the numerous microtumors found in patients. This difficulty is exacerbated by the fact that many of the widely disseminated tumors are small and even indistinguishable to the naked eye. In typical surgery of advanced stage ovarian cancer, large, easily identified tumors are first manually resected, followed by a laborious hunt for increasingly smaller tumors. Standard CRS procedure is to leave tumors in situ if they are deemed to be smaller than 1 cm in diameter (to treat with postoperative HIPEC later), or too close to a major blood vessel to be safely resected. These limitations often result in suboptimal CRS. While postoperative HIPEC can be effective at prolonging survival,^[42–44] ultimately, recurrence is common. Additionally, HIPEC is untargeted, it is likely to cause damage to all organs in the abdominal and pelvic cavity, and causes a high incidence of side effects (27–56% of cases^[45]) including intestinal fistula, intestinal obstruction, hematologic toxicity, and deep venous thrombosis. Despite significant effort and physical trauma to the patient, current treatments frequently prove inadequate, with frequent relapse and eventual death (EOC 5 year survival rate is below 30%).^[5–7]

In this study, we present a new intraoperative-theranostics strategy for advanced ovarian cancer with multiple tumor sites; utilizing C-GERTs to achieve intraoperative Raman detection-guided precise elimination of disseminated tumors with real-time and localized chemo-photothermal therapy. We believe that our C-GERT-based chemo-photothermal treatment is an excellent candidate to overcome the challenges of advanced stage ovarian cancer treatment, with significant advantages over other approaches. First, for tumor identification, the strongly enhanced fingerprint Raman spectra from GERTs allow us to identify tumors less than 0.1 cm in diameter within only 5 s, intraoperatively and without biopsy (vs 15 min for frozen section analysis). Clinical diagnosis could potentially use a cheap, easy to use handheld Raman scanner, for easy integration into clinical procedure. The ultra-photostability of GERTs allows for repeated identification of tumors.^[35] The accuracy of our diagnosis using GERTs is confirmed by the good agreement with the results of standard pathological diagnosis (**Figure 3d**). Second, the therapeutic effect of our C-GERT technique appears superior, with the potential to kill microtumors too small or too close to major blood vessels for resection; simplifying and improving treatment while minimizing the chance of relapse. Superior outcomes are demonstrated by the prolonged lifetimes and lower bioluminescence measured for mice in the C-GERTs + laser group (**Figures 4 and 5e**). Third, our treatment appears to have fewer harmful side effects than the clinical standard CRS + HIPEC. Clinically,

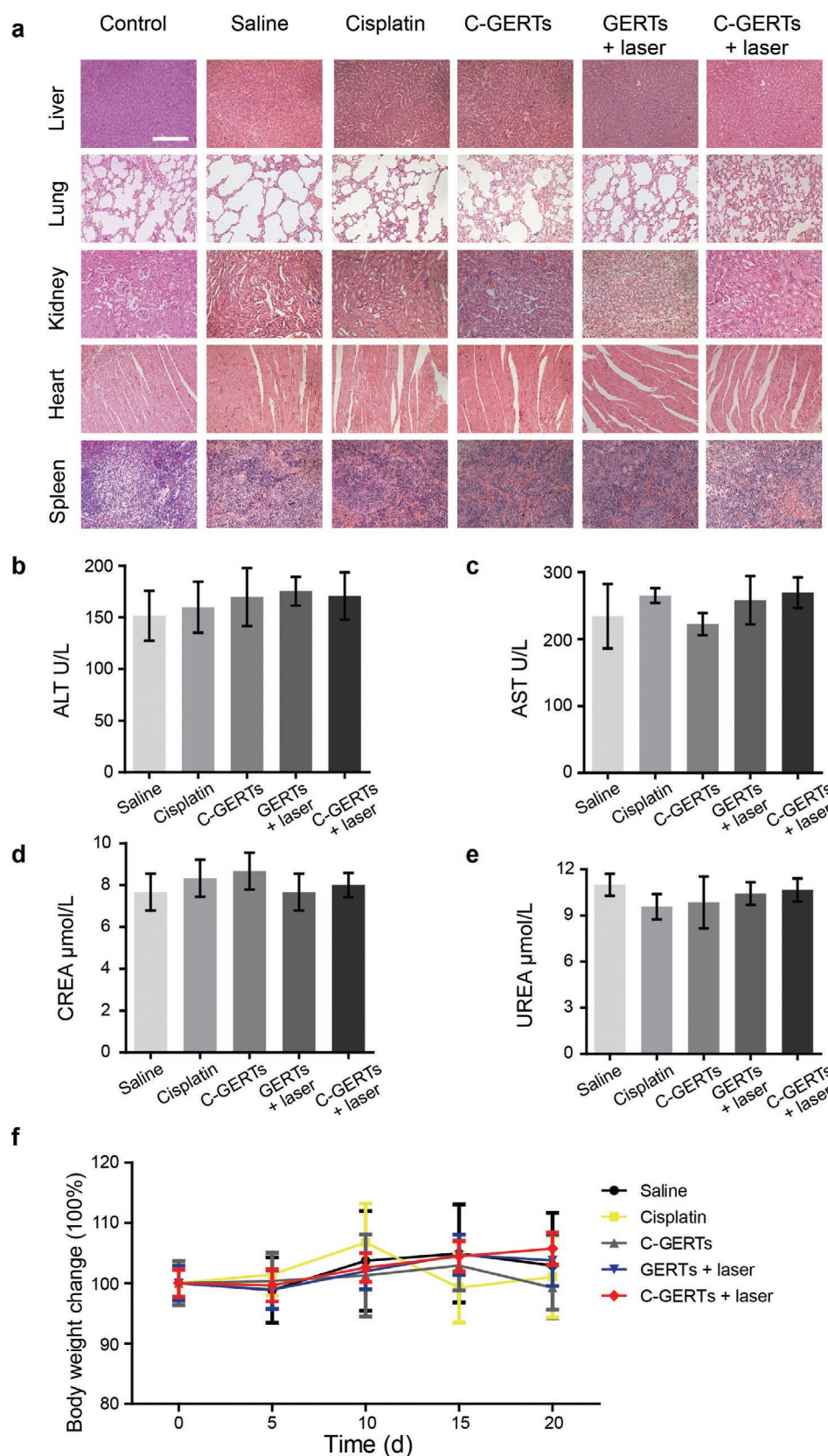


Figure 6. In vivo biocompatibility evaluation of different treatments. a) Histological analysis of major organs developed in mice with different treatments ≈ 20 days post therapy. Scale bar is 200 μm . b–e) Blood serum analysis of different groups of mice after treatment. ALT = alanin transaminase; AST = aspartate aminotransferase; CREA = creatinine. f) Body weight change of different groups of mice. Data are shown as mean and standard deviation.

for advanced stage ovarian cancer patients, surgeons commonly remove the primary ovary, whole uterus, double attachments, pelvic metastasis nodules, and even part of bowel if metastasis is diagnosed. Some patients need an artificial anus as a consequence of surgery. The mice in our C-GERTs + laser group retain basic integrity of their intestinal tissue, and postoperative symptoms of ileus are not found (Figure 6a). In addition to physical trauma from surgery, nephrotoxicity and hepatotoxicity of cisplatin is also a concern.^[46] Traditional clinical treatment requires multiple cisplatin administrations, which can inflict significant side effects on patients. In contrast, we only administer low-dose targeted cisplatin-loaded nanoparticles once, minimizing side effects while also avoiding those associated with HIPEC. Our results (Figure 6) show no evidence of biotoxicity of GERTs. Finally, our technique is the combination of Raman-based imaging, photothermal treatment, and chemotherapy with drug-loaded nanoparticles in one treatment, to create diagnostic and therapeutic potential greater than the sum of its parts. Using one multifunctional particle is highly desirable, to simplify procedure, minimize the time between detection and treatment, and avoid side effects. The signal of GERTs is also exceptionally good compared to traditional gold sphere nanoprobe, allowing clearer, quicker detection.^[36,47] In our experiments, different number of tumors may cause different surgery times, but we did not find that the extended anesthetic time had a dramatic impact on the therapeutic effect.

Furthermore, we emphasize the synergistic effect of our combined chemo- and photothermal therapies. While our results clearly show that our approach is significantly more effective than targeted cisplatin delivery alone (Figures 4 and 5), photothermal therapy alone can also be very effective, as evidenced by previous studies^[48,49] and our own results (GERTs + laser group). One way to increase the effectiveness of the photothermal effect for killing cancer cells is to simply increase the applied laser power or use a particle (such as gold nanorods) with a higher photothermal conversion efficiency.^[50,51] The trade-off is that excessive heating will damage surrounding healthy tissue, which beyond a point will result in negative outcomes. This was demonstrated in our preliminary experiments with GERTs and high laser powers of 5 W cm⁻² (Figure S8, Supporting Information). At such high laser powers, mice experienced intolerable damage to their intestines and quickly died. By combining cisplatin and photothermal therapy, we achieve equivalent cancer-killing ability at lower laser power, preventing excessive damage to surrounding tissue and significantly improving prognosis.

In summary, this is the first report to examine multifunctional C-GERTs as a new approach for real-time intraoperative accurate and sensitive detection and treatment of disseminated and unresectable tumors in vivo. The Raman detection-guided localized photothermal therapy and chemotherapy can kill cancer cells precisely, without damaging adjacent normal tissues.

4. Conclusion

In this paper, we present C-GERTs for intraoperative Raman-guided synergistic chemo-photothermal therapy of ovarian cancer, with the potential to be more effective, simpler, faster, and safer than both current clinical techniques and also other

targeted methods using chemotherapy/photothermal therapy alone. This potential is evidenced by our results in vitro and in vivo, which demonstrate superior tumor suppression, prevention of recurrence, and prolonged survival in mice. We have demonstrated that loading of GERTs with cisplatin does not impair their excellent Raman signal for sensitive imaging, that GERTs are effective nanoprobe for photothermal therapy, and that cisplatin-loaded C-GERTs can synergistically combine chemo- and photothermal therapies for more effective and safer treatment. Additionally, our results indicate no significant biotoxicity in major organs, nor any other side effects. We believe this is a promising therapy method to significantly improve prognosis for disseminated advanced stage ovarian cancer; a particularly challenging illness where current methods too frequently prove inadequate and impaired quality of life, recurrence, and death are too common.

5. Experimental Section

Materials: All materials were used as received without any further purification. Tetraethyl orthosilicate (TEOS), sodium hydroxide (NaOH), 3-aminopropyl triethoxysilane (APTES), *N,N*-dimethylformamide (DMF), succinic anhydride, dimethylsulfoxide (DMSO), and methanol were purchased from Sinopharm Chemical Reagent Co. Ltd. Cisplatin (cis-dichlorodiammineplatinum II) was obtained from Sigma-Aldrich. The ultrafine insulin syringes (1 mL) were purchased from Becton, Dickinson and Company (USA). The CCK-8 and calcein-AM/PI Double Stain Kit were purchased from Dojindo Laboratories (Kumamoto, Japan). Dulbecco's modified Eagle medium (DMEM)/high glucose medium, DMEM/F-12 (Ham) medium, penicillin-streptomycin mixture solution, fetal bovine serum (FBS), and 0.25% trypsin-ethylenediaminetetraacetic acid (EDTA) were purchased from Gibco Life Technologies (USA). Nanopure water (18.2 M Ω) was used for all experiments.

Instrumentation: TEM images of nanoprobe were collected on a JEM-2100F TEM (JEOL, Tokyo, Japan) operated at 200 kV. Tumor tissues were sectioned with EM UC7 Ultramicrotome (Leica, Solms, Germany) and observed used JEM-1230 TEM (JEON, Tokyo, Japan) operated at 80 kV. Fluorescence images were collected on a Leica inverted microscope (10 \times objective, 0.3 numerical aperture (NA)). The amount of cisplatin was measured by the atomic adsorption spectrometry via Polarized Zeeman AAS (Z-2000 Series, HITACHI, Japan). The Raman test was carried out on confocal Raman microscope (Horiba, Xplora INV).

Synthesis of GERTs: GERTs were synthesized according to the procedure described in the previous study.^[35] Briefly, Au cores were first synthesized using a seed-mediated process, then coated with Raman reporters and used as seeds to grow the Au shell. After that, a mesoporous silica coating was applied to GERTs according to Gorelikov and Matsuura's protocol with some modifications.^[52] The obtained GERT NPs (40 mL) were washed three times and then dispersed in 5 mL of water. NaOH solution (40 μ L, 0.1 M) was then added with stirring. Next, 50 μ L of 5% TEOS and 20 μ L of 5% APTES in methanol were added slowly to the solution while stirring gently. This procedure was repeated three times at 30 min intervals, and then the mixture was reacted for 24 h at 30 $^{\circ}$ C. The resulting products were collected by centrifugation and washed with ethanol (5 mL, three times) and DMF (5 mL, once). To the above products, succinic anhydride/DMF (5 mL, 0.4 M) was added and the mixture was stirred for 24 h. Finally, the resulting GERTs with carboxylic-functional groups on their surface were washed with DMF three times.

Cisplatin Loading and Releasing: Cisplatin (5 mg) was completely dissolved in 5 mL water-DMSO (1:1, v/v), and then the concentrated carboxylic-functionalized GERT (1 mL, 0.5×10^{-9} M) solution was added to the above cisplatin solution. After being stirred for 24 h in darkness at 45 $^{\circ}$ C, the resulting products were washed with water three times. After centrifugation, the supernatant was collected and the residual

cisplatin content measured by Polarized Zeeman AAS (HITACHI, Z-2000 Series) to determine the amount of loaded cisplatin. The drug content (Equation (1)) and loading efficiency (Equation (2)) were calculated as follows^[39]

$$\text{Drug content} = \frac{m_{\text{total}} - m_{\text{supernatant}}}{m_{\text{C-GERTs}}} \times 100\% \quad (1)$$

$$\text{Loading efficiency} = \frac{m_{\text{total}} - m_{\text{supernatant}}}{m_{\text{total}}} \times 100\% \quad (2)$$

where m_{total} is the total mass of cisplatin in the loading solution and $m_{\text{supernatant}}$ is the mass of cisplatin in the supernatant. $m_{\text{C-GERTs}}$ is the sum mass of GERTs and cisplatin added to the reaction bulb. Finally, the C-GERTs were washed with abundant water and dried in a vacuum oven overnight.

To study the cisplatin release profile, 3 mg of C-GERTs was dispersed in 3 mL of PBS (pH = 7.4) and then the suspension was transferred into a dialysis bag (3500 Da molecular weight cut off (MWCO), Sangon Biotech, China). The dialysis bag was then placed in 30 mL PBS and gently shaken at 37 °C. At the fixed time points, 1 mL of solution was taken out to test the amount of released cisplatin by Polarized Zeeman AAS (Z-2000 Series, HITACHI), and 1 mL of fresh medium was added to keep the volume constant. For the laser treatment group, after 24 h of dialysis, the C-GERTs were treated with the NIR laser (808 nm, 3 W cm⁻²) for 5 min, and then the solution was sampled, tested, and replaced in the same way.

Cell Cultures: The SKOV3_{luc} human ovarian cancer cells were obtained from Shanghai institute for Biological Sciences (Shanghai, China) and were stably transfected with the Luc gene. The SKOV3_{luc} cells were cultured at 37 °C under a humidified atmosphere of 5% CO₂ in DMEM medium with 10% FBS and 1% penicillin–streptomycin.

Cytotoxicity Assays In Vitro: SKOV3_{luc} cells (5 × 10³ per well) were plated in 96-well plates in triplicate. After 24 h, the medium was replaced with 100 μL complete growth medium containing GERTs with different concentrations (0.01 × 10⁻⁹, 0.02 × 10⁻⁹, 0.05 × 10⁻⁹, 0.1 × 10⁻⁹, and 0.2 × 10⁻⁹ M) and incubated for further 24, 48, and 72 h. Cell viability was measured by CCK-8 assay according to the manufacturer's instructions. At least three independent experiments were done.

Combined Chemo-Photothermal Therapy on Tumor Cells: To demonstrate the effects of combined chemo-photothermal therapy of the probes on tumor cells, SKOV3_{luc} cells (5 × 10³ per well) were seeded in 96-well plates and incubated with GERT or C-GERT nanoprobe with the concentration of 0.1 × 10⁻⁹ M. After 24 h, the cells were washed twice with PBS and treated with the NIR laser (808 nm, 3 W cm⁻²) for 5 min. After laser treatment, the cells were cultured for 6 h, and cell viability was evaluated using the CCK-8 assay and calcein-AM/PI staining.

Advanced Ovarian Cancer Model and In Vivo Therapy: All animal experiments were approved by the animal care committee of the Renji Hospital, School of Medicine, Shanghai Jiao Tong University. SKOV3_{luc} cells (2.8 × 10⁶) were suspended in 250 μL PBS and inoculated by intraperitoneal injection (i.p.) into 5 to 7 week old female nude mice, 10 mice in each group.^[53] Two weeks after inoculation, the experiments were carried out. The mice were divided into five groups ($n = 10$ each group): the first group (saline group) was given a tail vein injection of saline (200 μL per mice) and intraoperatively treated with NIR radiation; the second group (cisplatin group) was injected with cisplatin (5 mg kg⁻¹); the third group (C-GERT group) was injected with C-GERT nanoparticles containing an equivalent dose of free cisplatin (200 μL, 1 × 10⁻⁹ M); the fourth group (GERTs + laser group) was injected with GERTs (200 μL, 1 × 10⁻⁹ M) and intraoperatively treated with NIR radiation; the last group (C-GERTs + laser group) was injected with C-GERT nanoparticles and treated with NIR radiation. 24 h after tail vein injection, all mice were anesthetized and underwent aseptic laparotomy surgery. The disseminated tumors in the abdominal cavity were imaged with the Raman system (20 mW, 10× objective lens) with a 785 nm laser, a macrolaser spot of 300 × 300 μm² with DuoScan scanning mode, and 5 s integration time. After identifying the tumor foci from their GERTs

Raman signals, NIR laser treatment (3 W cm⁻², 808 nm) was applied for 5 min to all tumor locations except for those located on the intestinal wall; for tumors on the intestinal wall, the irradiation time was decreased to 3 min to minimize the effect on intestinal peristalsis.

Therapeutic Efficiency and Systemic Toxicity: One day before and 4, 10, 16, and 20 days after operation, tumor growth was monitored by bioluminescence after i.p. injection of 3 mg of D-luciferin (GoldBio Technology, St. Louis, MO) in 200 μL PBS with an IVIS Spectrum (Xenogen, Shrewsbury, MA). 20 days after operation, 5 mice of each group were euthanized with CO₂ and the number of visible tumors in the cavity was counted and weighted. Hematoxylin eosin (H&E) staining of major organs (heart, liver, spleen, lungs, and kidneys), nephrotoxicity and hepatotoxicity detection (the concentrations of ALT, AST, CREA, and urea in plasma) were carried out to evaluate the biocompatibility of the probes. The body weights were measured every 2 days over a 20 day period to evaluate the systemic toxicity. Another 3 mice were selected from each group to evaluate the overall survival until 30 days.

Statistical Analysis: Results were analyzed using GraphPad prism 5 software. Group comparisons were performed using one-way analysis of variance (ANOVA) and p values of less than 0.05 indicated significant differences. Unpaired Student's t -test was used between two-group comparisons. Data were expressed as the mean ± standard deviation (SD).

Supporting Information

Supporting Information is available from the Wiley Online Library or from the author.

Acknowledgements

Y.Z. and Z.L. contributed equally to this work. The authors gratefully acknowledge the financial support from the National Natural Science Foundation of China (Grant Nos. 81571763, 81622026, 81472426, and 21375087), the Shanghai Municipal Commission of Health and Family Planning (Grant Nos. 15GWZK0701 and 2017ZZ02016), the National Key R&D Program of China (Grant No. 2016YFC1302900), the Shanghai Jiao Tong University (Grant Nos. YG2016MS51 and YG2017MS54), and the Shanghai Key Laboratory of Gynecological Oncology.

Conflict of Interest

The authors declare no conflict of interest.

Keywords

intraoperative, nanoprobe, surface enhanced Raman scattering, therapy, tumors

Received: March 16, 2018

Revised: May 8, 2018

Published online:

- [1] D. Jelovac, D. K. Armstrong, *Ca-Cancer J. Clin.* **2011**, *61*, 183.
- [2] A. Berkenblit, S. A. Cannistra, *J. Reprod. Med.* **2005**, *50*, 426.
- [3] L. A. Torre, F. Bray, R. L. Siegel, J. Ferlay, J. Lortet-Tieulent, A. Jemal, *Ca-Cancer J. Clin.* **2015**, *65*, 87.
- [4] G. C. Jayson, E. C. Kohn, H. C. Kitchener, J. A. Ledermann, *Lancet* **2014**, *384*, 1376.

- [5] S. Vaughan, J. I. Coward, R. C. Bast Jr., A. Berchuck, J. S. Berek, J. D. Brenton, G. Coukos, C. C. Crum, R. Drapkin, D. Etemadmoghadam, M. Friedlander, H. Gabra, S. B. Kaye, C. J. Lord, E. Lengyel, D. A. Levine, I. A. McNeish, U. Menon, G. B. Mills, K. P. Nephew, A. M. Oza, A. K. Sood, E. A. Stronach, H. Walczak, D. D. Bowtell, F. R. Balkwill, *Nat. Rev. Cancer* **2011**, 11, 719.
- [6] D. D. Bowtell, S. Bohm, A. A. Ahmed, P. J. Aspuria, R. C. Bast Jr., V. Beral, J. S. Berek, M. J. Birrer, S. Blagden, M. A. Bookman, J. D. Brenton, K. B. Chiappinelli, F. C. Martins, G. Coukos, R. Drapkin, R. Edmondson, C. Fotopoulou, H. Gabra, J. Galon, C. Gourley, V. Heong, D. G. Huntsman, M. Iwanicki, B. Y. Karlan, A. Kaye, E. Lengyel, D. A. Levine, K. H. Lu, I. A. McNeish, U. Menon, S. A. Narod, B. H. Nelson, K. P. Nephew, P. Pharoah, D. J. Powell Jr., P. Ramos, I. L. Romero, C. L. Scott, A. K. Sood, E. A. Stronach, F. R. Balkwill, *Nat. Rev. Cancer* **2015**, 15, 668.
- [7] K. A. Lowe, V. M. Chia, A. Taylor, C. O'Malley, M. Kelsh, M. Mohamed, F. S. Mowat, B. Goff, *Gynecol. Oncol.* **2013**, 130, 107.
- [8] M. Matz, M. P. Coleman, M. Sant, M. D. Chirlaque, O. Visser, M. Gore, C. Allemani, *Gynecol. Oncol.* **2017**, 144, 405.
- [9] S. M. Eisenkop, R. L. Friedman, H. J. Wang, *Gynecol. Oncol.* **1998**, 69, 103.
- [10] R. E. Bristow, R. S. Tomacruz, D. K. Armstrong, E. L. Trimble, F. J. Montz, *J. Clin. Oncol.* **2002**, 20, 1248.
- [11] M. E. L. van der Burg, M. van Lent, M. Buyse, A. Kobierska, N. Colombo, G. Favalli, A. J. Lacave, M. Nardi, J. Renard, S. Pecorelli, *N. Engl. J. Med.* **1995**, 332, 629.
- [12] I. Ramirez, H. Chon, S. Apte, *Cancer Control* **2011**, 18, 22.
- [13] C. Gerestein, D. van der Spek, M. Eijkemans, J. Bakker, G. Kooi, C. Burger, *Int. J. Gynecol. Cancer* **2009**, 19, 1511.
- [14] R. L. Coleman, B. J. Monk, A. K. Sood, T. J. Herzog, *Nat. Rev. Clin. Oncol.* **2013**, 10, 211.
- [15] A. N. Fader, P. G. Rose, *J. Clin. Oncol.* **2007**, 25, 2873.
- [16] E. Lengyel, *Am. J. Pathol.* **2010**, 177, 1053.
- [17] S. Kaur, H. A. Kenny, S. Jagadeeswaran, M. R. Zillhardt, A. G. Montag, E. Kistner, S. D. Yamada, A. K. Mitra, E. Lengyel, *Am. J. Pathol.* **2009**, 175, 2184.
- [18] C. Grimm, P. Harter, P. F. Alesina, S. Prader, S. Schneider, B. Ataseven, B. Meier, V. Brunkhorst, J. Hinrichs, C. Kurzeder, F. Heitz, A. Kahl, A. Traut, H. T. Groeben, M. Walz, A. du Bois, *Gynecol. Oncol.* **2017**, 146, 498.
- [19] G. Cormio, C. Rossi, A. Cazzolla, L. Resta, G. Loverro, P. Greco, L. Selvaggi, *Int. J. Gynecol. Cancer* **2003**, 13, 125.
- [20] K. M. Nieman, H. A. Kenny, C. V. Penicka, A. Ladanyi, R. Buell-Gutbrod, M. R. Zillhardt, I. L. Romero, M. S. Carey, G. B. Mills, G. S. Hotamisligil, S. D. Yamada, M. E. Peter, K. Gwin, E. Lengyel, *Nat. Med.* **2011**, 17, 1498.
- [21] R. F. Ozols, B. N. Bundy, B. E. Greer, J. M. Fowler, D. Clarke-Pearson, R. A. Burger, R. S. Mannel, K. DeGeest, E. M. Hartenbach, R. Baergen, *J. Clin. Oncol.* **2003**, 21, 3194.
- [22] L. Galluzzi, L. Senovilla, I. Vitale, J. Michels, I. Martins, O. Kepp, M. Castedo, G. Kroemer, *Oncogene* **2012**, 31, 1869.
- [23] B. Stordal, N. Pavlakis, R. Davey, *Cancer Treat. Rev.* **2007**, 33, 688.
- [24] A. Di Giorgio, E. Naticchioni, D. Biacchi, S. Sibio, F. Accarpio, M. Rocco, S. Tarquini, M. Di Seri, A. Ciardi, D. Montruccoli, P. Sammartino, *Cancer* **2008**, 113, 315.
- [25] M. Deraco, S. Kusamura, S. Virzi, F. Puccio, A. Macri, C. Famulari, M. Solazzo, S. Bonomi, D. R. Iusco, D. Baratti, *Gynecol. Oncol.* **2011**, 122, 215.
- [26] J. Spiliotis, E. Halkia, E. Lianos, N. Kalantzi, A. Grivas, E. Efstathiou, S. Giassas, *Ann. Surg. Oncol.* **2015**, 22, 1570.
- [27] C. W. Helm, *Oncologist* **2009**, 14, 683.
- [28] A. D. Newton, E. K. Bartlett, G. C. Karakousis, *J. Gastrointest. Oncol.* **2016**, 7, 99.
- [29] M. Kircher, A. de la Zerda, J. Jokerst, C. Zavaleta, P. Kempen, E. Mittra, K. Pitter, R. Huang, C. Campos, F. Habte, R. Sinclair, C. Brennan, I. Mellinghoff, E. Holland, S. Gambhir, *Nat. Med.* **2012**, 18, 829.
- [30] C. Andreou, S. Kishore, M. Kircher, *J. Nucl. Med.* **2015**, 56, 1295.
- [31] S. Harmsen, R. Huang, M. A. Wall, H. Karabeber, J. M. Samii, M. Spaliviero, J. R. White, S. Monette, R. O'Connor, K. L. Pitter, S. A. Sastra, M. Saborowski, E. C. Holland, S. Singer, K. P. Olive, S. W. Lowe, R. G. Blasberg, M. F. Kircher, *Sci. Transl. Med.* **2015**, 7, 271ra7.
- [32] H. Karabeber, R. Huang, P. Iacono, J. M. Samii, K. Pitter, E. C. Holland, M. F. Kircher, *ACS Nano* **2014**, 8, 9755.
- [33] C. Andreou, V. Neuschmelting, D.-F. Tschaharganeh, C.-H. Huang, A. Oseledchik, P. Iacono, H. Karabeber, R. R. Colen, L. Mannelli, S. W. Lowe, M. F. Kircher, *ACS Nano* **2016**, 10, 5015.
- [34] A. Oseledchik, C. Andreou, M. A. Wall, M. F. Kircher, *ACS Nano* **2017**, 11, 1488.
- [35] Y. Zhang, Y. Qiu, L. Lin, H. Gu, Z. Xiao, J. Ye, *ACS Appl. Mater. Interfaces* **2017**, 9, 3995.
- [36] L. Lin, H. Gu, J. Ye, *Chem. Commun.* **2015**, 51, 17740.
- [37] L. Lin, Z. Liu, X. Li, H. Gu, J. Ye, *Nanoscale* **2017**, 9, 2213.
- [38] J. Gu, S. Su, Y. Li, Q. He, J. Zhong, J. Shi, *J. Phys. Chem. Lett.* **2010**, 1, 3446.
- [39] D. K. Roper, W. Ahn, M. Hoepfner, *J. Phys. Chem. C* **2007**, 111, 3636.
- [40] H. Maeda, *Bioconjugate Chem.* **2010**, 21, 797.
- [41] L. Brannon-Peppas, J. O. Blanchette, *Adv. Drug Delivery Rev.* **2004**, 56, 1649.
- [42] D. K. Armstrong, B. Bundy, L. Wenzel, H. Q. Huang, R. Baergen, S. Lele, L. J. Copeland, J. L. Walker, R. A. Burger, *N. Engl. J. Med.* **2006**, 354, 34.
- [43] P. A. Cascales-Campos, J. Gil, E. Gil, E. Feliciangeli, A. González-Gil, J. J. Parrilla, P. Parrilla, *Ann. Surg. Oncol.* **2014**, 21, 2383.
- [44] T. Safran, D. Grisaru, M. Inbar, S. Abu-Abeid, D. Dayan, D. Matcayevsky, A. Weizman, J. Klausner, *J. Surg. Oncol.* **2014**, 110, 661.
- [45] P. Shen, E. A. Levine, J. Hall, D. Case, G. Russell, R. Fleming, R. McQuellon, K. R. Geisinger, B. W. Loggie, *Arch. Surg.* **2003**, 138, 26.
- [46] M. Veslemes, D. Antoniou, N. Georgatou, P. Giamboudakis, J. Dimitroulis, K. Katis, G. Stathopoulos, *Anticancer Res.* **2005**, 25, 2991.
- [47] J. Li, J. Ye, C. Chen, Y. Li, N. Verellen, V. Moshchalkov, L. Lagae, P. V. Dorpe, *ACS Photonics* **2015**, 2, 425.
- [48] P. M. Peiris, A. Abramowski, J. McGinnity, E. Doolittle, R. Toy, R. Gopalakrishnan, S. Shah, L. Bauer, K. B. Ghaghada, C. Hoimes, S. M. Brady-Kalnay, J. P. Basilion, M. A. Griswold, E. Karathanasis, *Cancer Res.* **2015**, 75, 1356.
- [49] C. Ayala-Orozco, C. Urban, S. Bishnoi, A. Urban, H. Charron, T. Mitchell, M. Shea, S. Nanda, R. Schiff, N. Halas, A. Joshi, *J. Controlled Release* **2014**, 191, 90.
- [50] H. Chen, L. Shao, T. Ming, Z. Sun, C. Zhao, B. Yang, J. Wang, *Small* **2010**, 6, 2272.
- [51] Z. Zha, X. Yue, Q. Ren, Z. Dai, *Adv. Mater.* **2013**, 25, 777.
- [52] I. Gorelikov, N. Matsuura, *Nano Lett.* **2008**, 8, 369.
- [53] K. Yamanouchi, T. Ohta, Z. Liu, Y. Oji, H. Sugiyama, V. Shridhar, S. Matsumura, T. Takahashi, K. Takahashi, H. Kurachi, *Transl. Oncol.* **2014**, 7, 580.